01 Jan 2008

Energy Harvesting Using Piezoelectric Materials and High Voltage Scavenging Circuitry

Shahab Mehraeen

Jagannathan Sarangapani
Missouri University of Science and Technology, sarangap@mst.edu

Keith Corzine
Missouri University of Science and Technology

Recommended Citation

S. Mehraeen et al., "Energy Harvesting Using Piezoelectric Materials and High Voltage Scavenging Circuitry," *Proceedings of the IEEE International Conference on Industrial Technology, 2008*, Institute of Electrical and Electronics Engineers (IEEE), Jan 2008.
The definitive version is available at https://doi.org/10.1109/ICIT.2008.4608554

Energy Harvesting Using Piezoelectric Materials and High Voltage Scavenging Circuitry[1]

Shahab Mehraeen, S. Jagannathan, and Keith Corzine

Abstract - **Piezoelectric transducers are increasingly being used to harvest energy from environmental vibrations in order to power remote sensors or to charge batteries that power the sensors. In this paper, two modifications have been analyzed and tested to increase the harvested electrical power from a vibrating piezoelectric material. First, the voltage inversion method, which has recently been used in piezoelectric-based energy harvesting, and that shapes the voltage to be in phase with current in order to increase the harvested power is reviewed. By injecting additional current, a new voltage inversion scheme, referred as voltage compensation scheme, is introduced. This new scheme provides more than 14% increase in harvesting power over the parallel inversion method (parallel SSHI) alone and more than 50% in the case of series inversion method (series SSHI) alone. Second, the tapered cantilever beams were shown to be more effective in generating a uniform strain profile over rectangular and trapezoidal beams if they are precisely shaped. Using this modification, it is shown that a 300% increase in harvested power over available methods in the literature is obtainable.**

***Index Terms* –. Energy Harvesting, Piezoelectric, Cantilever beam**

I. Introduction

The demand for wireless sensors and portable electronic devices has been increasing in recent years. One of the most important applications is remote sensing and embedded prognostics. As wireless devices are becoming omnipresent, batteries are used to power these embedded devices. However, due to their low durability, batteries have to be replaced periodically. This procedure is costly especially for sensors that monitor remote structures. Possible examples of such applications include health monitoring of earthmoving equipment and bridges for which continuous data gathering is essential. Therefore, for many prognostic applications, it is of paramount importance to replace batteries with a more durable source of energy. One of the most applicable ways to solve this problem is to harvest energy from the environment. Energy harvesting is defined as the conversion of ambient energy into a usable electrical form. If the scavenged energy from the surrounding is insufficient to power the sensor, at least the battery lifetime can be extended. Additionally, the size of the batteries could be reduced through energy harvesting. Among available energy harvesting methodologies, piezoelectric-based approach was chosen because of abundant vibration accessibility and harvesting productivity of piezoelectric materials [1].

Direct connection of the load to the piezoelectric material is not the most efficient way of harvesting energy. A typical energy harvesting scheme consists of a piezoelectric material bonded to a cantilever beam, voltage inversion circuitry, rectifier, power converter for conditioning, and the load. It has been shown that conditioning the voltage can increase the scavenged power form a piezoelectric material [2-3]. Moreover, different voltage inversion techniques [4-5] have been proposed to shape the voltage in order to increase the voltage and power factor from the piezoelectric material and as a result to increase the harvested power. Although the shaped voltage in voltage inversion techniques increases the harvested power noticeably, it is not the optimal voltage.

In this paper a new method is introduced to shape the voltage in order to achieve the optimal voltage waveform in piezoelectric-based power harvesting.

II. Piezoelectric Electromechanical Model

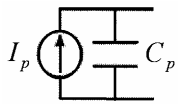

Fig.1. Equivalent electrical circuit of a PZT.

A vibrating piezoelectric (PZT) device differs from a typical electrical power source since its internal impedance is capacitive rather than inductive in nature. The mathematical equations for a piezoelectric material are given by [6] as $\delta = \frac{\sigma}{Y} + dE$ and $D = \varepsilon E + d\sigma$ where δ is mechanical strain, σ is mechanical stress, Y is material Young's modulus, d is the piezoelectric strain coefficient, E is the electrical field, D is charge density, and ε is the dielectric constant of the piezoelectric material. Under sinusoidal vibration, the second equation can be transformed into a more convenient form as

[1] Authors are with Department of Electrical and Computer Engineering, Missouri University of Science and Technology, 1870 Miner Circle, Rolla, MO 65409. Contact author: sm347@mst.edu.

Research Supported in part by NSF I/UCRC on Intelligent Maintenance Systems award.

978-1-4244-1706-3/08/$25.00 ©2008 IEEE.

$I = i_P - C_P \dot{V}$ where I is the output current, $i_p = I_P \sin(\omega t)$ is the PZT polarization current with peak value given by I_p, ω is the frequency, C_P is the PZT capacitance, and V is the PZT terminal voltage. A simple schematic circuitry for PZT is depicted in Fig. 1.

III. Voltage Inversion Techniques

Voltage inversion techniques [4-5], referred as synchronized switch harvesting on inductor (SSHI), are the most powerful available techniques to boost the output electric power in a piezoelectric material which is subjected to alternating strain. In these techniques, the voltage of the piezoelectric clamped capacitor is inverted through an inductor each time the polarization current changes sign. The main idea in the parallel SSHI technique, as shown in Fig. 2a, is to shape the piezoelectric voltage waveform in order to force it to be in phase with the polarization current so that the power factor can be enhanced. Additionally, the magnitude of DC voltage is increased as a result of the voltage inversion and this would result in an increase in scavenged power. In order to make the voltage inversion technique functional, the electronic switching circuitry utilized only consumes 5% consumption of total harvested power [4]. Although the available voltage inversion techniques harvest power, they are not optimal due to the need for a square voltage waveform. Generation of a square voltage waveform requires very fast switching techniques and a large inductor which in turn increases the complexity and size of the inverting hardware especially when high voltages (i.e. $V > 100$) are involved.

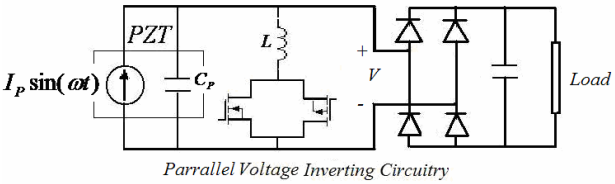

Fig. 2 (a) PZT Parallel voltage inversion topology.

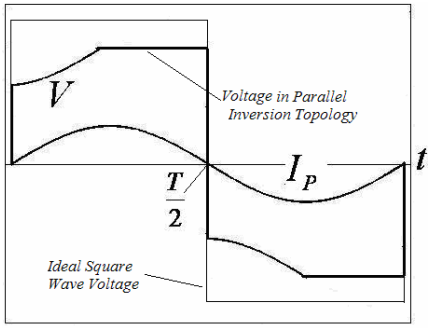

Fig. 2 (b) PZT voltage and current waveforms.

The series voltage inversion technique works in a similar way as the parallel technique except that the load is connected in series with the inductor and switches as depicted in Fig. 3a in order to transfer the power during the switching time.

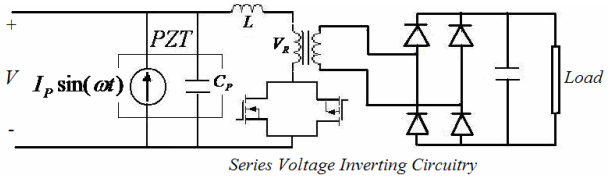

Fig. 3 (a) PZT Series voltage inversion topology.

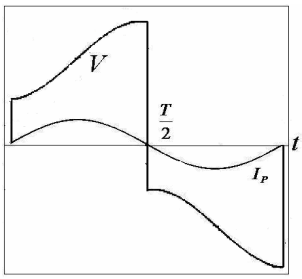

Fig. 3 (b) PZT voltage and current waveforms

Although original series voltage inversion has been proven to be less productive than the parallel technique [5] for its lower average output voltage, the former has the merit of feeding low voltages through the transformer as illustrated in Fig. 3a which in turn avoids a large voltage difference between PZT output and low-voltage application needs. It is not generally advisable to have a high voltage difference between the harvester and the load to avoid impractically small duty cycles in the power converter that steps down the voltage to meet the load requirements [2] .

Recall that in a constant vibration environment, the amplitude of piezoelectric polarization current I_P is constant. It is also important to note that if the generated voltage is low, accordingly a low power is harvested. In all the power boosting methods described above, due to the dissipations involved in switching hardware typically built using solid-state switches and inductors, the magnitude of the output voltage is less than what it would be in a lossless inversion. The voltage drop is significantly high in high voltage/power applications due to high switching and core losses. To mitigate this problem, the following method is introduced which contributes to an increase in harvested power in a voltage inverting power boosting method. The proposed scheme injects current to the piezoelectric material after each voltage inversion in order to increase the voltage level.

IV. Proposed Voltage Compensation Scheme

The proposed voltage compensation scheme can be introduced both with parallel and series inversion techniques as given next.

A. Voltage compensation in parallel inversion method

Fig.4a represents the proposed two-stage voltage compensating topology in which switches B1 and C1 are synchronized with switch A1 and switches B2 and C2 are synchronized with switch A2. Increasing the number of stages provides more output power as will be described later;

however, it results in more complex circuitry. The new switches are synchronized with the original inverting switches by using an adequate delay in order to end the inversion process and establish the new voltage in the original power inversion circuitry. The voltage compensation switches are then closed consecutively to allow the transfer of energy to the piezoelectric clamped capacitor thus compensating the voltage in each half cycle. Since it is always necessary to have a converter to deliver the power to the load [2], a multi output converter can be utilized to provide the compensation voltages as well as load voltage. A typical piezoelectric waveform during voltage inversion is depicted in Fig. 4b for this topology.

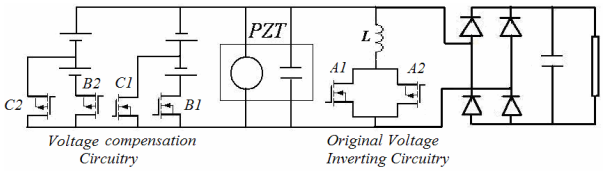

Fig. 4 (a) Parallel power compensation topology.

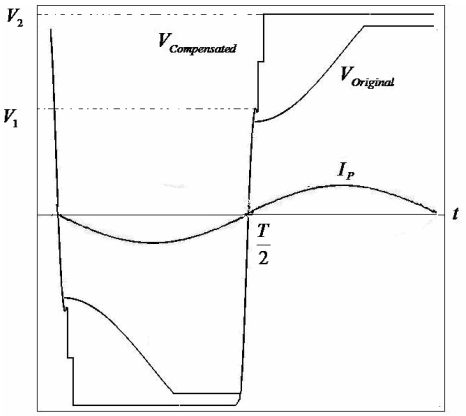

Fig. 4 (b) Voltage waveforms in original parallel voltage inverting method and in voltage compensation method with two-step compensation.

Using the proposed topology the injected energy to the piezoelectric clamping capacitor, the dissipated energy during voltage compensation, and the total harvested energy under the new voltage level can be calculated as given next. Noting that the voltage inversion process is nothing but a half-cycle underdamped series RLC oscillation with a series voltage source, one can easily show that

$$V_{C\min} = V_L + \frac{(V_C(0) - V_L)}{\varpi\sqrt{LC_P}} e^{-\bar{\sigma}t} \sin(\varpi t + \theta) \quad (1)$$

where $\varpi t + \theta = \pi$, $\bar{\sigma}$ and ϖ are the real and imaginary parts of RLC eigenvalues, and V_L is the series dc voltage. Setting $V_L = 0$ for parallel inversion and designating $\gamma = \left|\frac{V_{C\min}}{V_C(0)}\right| = \left|\frac{V_1}{V_2}\right|$, where V_2 and V_1 are the voltages before and after the switching, respectively, one finds that the change in stored energy in the clamped capacitor during current injection is given by

$$E_C = \frac{1}{2}C_p(V_2^2 - V_1^2) = \frac{1}{2}C_pV_2^2(1-\gamma^2). \quad (2)$$

This direct charging involves some energy dissipation regardless of the amount of path resistance which is given by

$$E_{DISS} = \frac{1}{2\alpha}C_p(V_2 - V_1)^2 = \frac{1}{2\alpha}C_pV_2^2(1-\gamma)^2 \quad (3)$$

where the parameter α is the number of equally apart voltage steps from V_1 to V_2. The independency of dissipation from path resistance relaxes the need for high speed switching and thus allowing simple switching techniques to be more useful. The harvested energy during a half-cycle at constant voltage V_2 is given by

$$E_H = \int_0^{T/2} I_P \sin(\omega t)V_2 dt = \frac{2I_PV_2}{\omega} \quad (4)$$

where $I_P \sin(\omega t)$ is the polarization current provided by piezoelectric material in a sinusoidal mechanical motion. The net output energy, which is defined as the difference between harvested and consumed energy becomes

$$\Delta E = E_H - E_C - E_{DISS} = \frac{2I_PV_2}{\omega} - \frac{1}{2}C_pV_2^2(1-\gamma^2) - \frac{1}{2\alpha}C_pV_2^2(1-\gamma)^2 \quad (5)$$

Combining the last two terms in (4) yields

$$\Delta E = \frac{2I_PV_2}{\omega} - \frac{1}{2\alpha}C_pV_2^2[1+\alpha(1-\gamma^2)+\gamma(\gamma-2)] = \frac{2I_PV_2}{\omega} - KC_pV_2^2 \quad (6)$$

where $K = \frac{1+\alpha(1-\gamma^2)+\gamma(\gamma-2)}{2\alpha}$ reflects the specifications of the voltage inverting and compensating circuitries. The maximum net energy ΔE_{OPT} will take place in the optimum output voltage V_{2OPT} as presented

$$\frac{d\Delta E}{dV_2} = 0 \Rightarrow V_{2OPT} = \frac{I_P}{K\omega C_P} \text{ and } \Delta E_{MAX} = \frac{I_P^2}{K\omega^2 C_P}. \quad (7)$$

This yields the maximum output power

$$P_{MAX} = \frac{\Delta E_{MAX}}{T/2} = \frac{I_P^2}{K\pi\omega C_P} \quad (8)$$

It's apparent that $\alpha \to \infty \Rightarrow P_{MAX} \to \frac{2}{1+\gamma}P_{1MAX}$ where P_{1MAX} is the maximum power produced by the original parallel voltage inverting method and is given as [5]

$$P_{1MAX} = \frac{I_P^2}{\pi C_P\omega(1-\gamma)}.$$

Thus, as γ approaches 1, the generated power in the new scheme approaches that of original parallel inversion method.

One important consequence of (8) is that for a one-step voltage compensation (i.e. $\alpha = 1$), the maximum output power is equal to the maximum output power generated from the original parallel voltage inversion technique. As a result, for parallel voltage inversion method at least two-step compensation is desirable.

According to (8), for $\alpha = 2$ and $\gamma = 0.5$, which is practically feasible in high voltage applications, an increase of 14% over the original parallel voltage inversion technique will be observed.

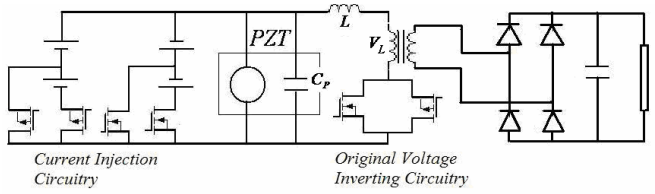

Fig. 5 (a) Series power compensation topology.

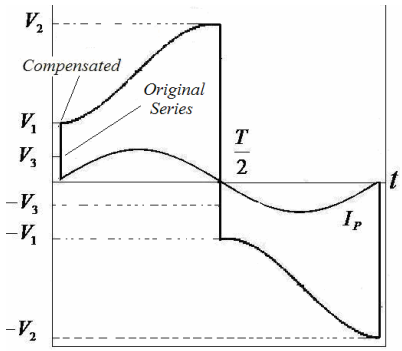

Fig. 5 (b) Voltage levels in original series voltage inverting method and in voltage compensation method.

B. Voltage compensation in series inversion method

The current injection topology as well as the original and compensated voltage levels for series inversion technique is depicted in Fig. 5. The voltage starts to fall from V_2 to $-V_3$ as a result of inversion and during the transfer of energy to the load. At the end of inversion, current is injected into the piezoelectric clamping capacitor C_P and increases the voltage to $|-V_1|$. Then, all the switches are opened and the piezoelectric polarization current source starts to transfer charge to the clamping capacitor. Following the same procedure as in the case of parallel inversion method, the given energy to the piezoelectric clamping capacitor, the dissipated energy during current injection, and the total harvested energy according to the new voltage level have to be calculated. The change in the stored energy in the clamping capacitor and the dissipated energy during current injection in each half cycle are given by

$$E_C = \frac{1}{2} C_p (V_1^2 - V_3^2)$$
$$E_{DISS} = \frac{1}{2\alpha} C_p (V_1 - V_3)^2 \qquad (9)$$

where the parameter α is the number of equally apart voltage steps from V_1 to V_3. Also, the new harvested energy during the same half cycle will be

$$E_H = QV_L = C_P (V_2 + V_3) V_L \qquad (10)$$

where V_L is the DC voltage across the load. Recalling $-V_3 = V_L + (-V_2 + V_L)\gamma$ from equation (1) where $\gamma = \left| \frac{V_3 + V_L}{V_2 - V_L} \right|$ and $V_2 = V_1 + \frac{2I_P}{C_P \omega}$ from the piezoelectric model, one will obtain the voltage prior to compensation as

$$V_3 = -V_L(1+\gamma) + V_1\gamma + \frac{2I_P\gamma}{C_P\omega} \qquad (11)$$

Plugging (11) into set of equations (9) and (10) gives the net output energy in a half-cycle for series voltage compensation as

$$\Delta E = E_H - E_C - E_{Diss} =$$
$$C_P(1+\gamma)[V_1 + \frac{2I_P}{C_P\omega} - V_L]V_L -$$
$$\frac{C_P}{2\alpha}\left((\alpha+1)V_1^2 - (\alpha-1)\left[-V_L(1+\gamma) + V_1\gamma + \frac{2I_P\gamma}{C_P\omega} \right]^2 \right. \qquad (12)$$
$$\left. - 2V_1\left[-V_L(1+\gamma) + V_1\gamma + \frac{2I_P\gamma}{C_P\omega} \right] \right)$$

The optimization of ΔE with respect to V_1 and V_R results in solving $\frac{\partial \Delta E}{\partial V_1} = 0$ and $\frac{\partial \Delta E}{\partial V_L} = 0$ which in turn yields the set of equations

$$b_1 V_L + b_2 V_1 = a_1$$
$$b_2 V_L + b_3 V_1 = a_2 \qquad (13)$$

where the parameters are

$$b_1 = -\left(2C_P(1+\gamma) - \frac{C_P}{\alpha}(\alpha-1)(1+\gamma)^2 \right)$$
$$b_2 = C_P(1+\gamma) - \frac{C_P}{\alpha}(\alpha-1)(1+\gamma)\gamma - \frac{C_P}{\alpha}(1+\gamma)$$
$$b_3 = -\left(\frac{C_P}{\alpha}(\alpha+1-2\gamma) - \frac{C_P}{\alpha}(\alpha-1)\gamma^2 \right)$$
$$a_1 = -\left(\frac{2(1+\gamma)I_P}{\omega} - \frac{2}{\alpha\omega}(\alpha-1)(1+\gamma)\gamma I_P \right) \qquad (14)$$
$$a_2 = -\left(\frac{2}{\alpha\omega}(\alpha-1)\gamma^2 I_P + \frac{2}{\alpha\omega}\gamma I_P \right)$$

As α approaches infinity, and in the case that $V_3 = -V_1$, the equations (9) are relaxed and with $V_L = \frac{V_1}{2} + \frac{I_P}{C_P\omega}$ as optimal load voltage, the maximum net output power becomes

$$P_{MAX} = \frac{I_P^2(1+\gamma)}{\pi C_P \omega} + \frac{\omega C_P(1+\gamma)}{4\pi} V_1^2 + \frac{(1+\gamma)}{\pi} I_P V_1 \qquad (15)$$

A careful look at (15) reveals that the net output power in the series inversion method can be arbitrarily high regardless of the amount of γ as long as the number of compensation steps, if practical, is large enough.

The relationship between the optimal voltages and maximum power for a one-step voltage compensation will be simplified as $\frac{d\Delta E}{dV_1} = 0 \Rightarrow V_{1OPT} = \frac{I_P \gamma}{C_P(1-\gamma)\omega}$, $\frac{d\Delta E}{dV_R} = 0 \Rightarrow V_{R\_OPT} = \frac{I_P}{C_P \omega}$, and

$$\Delta E_{MAX} = \frac{I_P^2 \gamma^2}{C_P(1-\gamma)\omega^2} + \frac{I_P^2(1+\gamma)}{C_P \omega^2}. \quad (16)$$

and the net output power will be given by

$$P_{MAX} = \frac{\Delta E_{MAX}}{T/2} = \frac{I_P^2}{\pi C_P(1-\gamma)\omega} \quad (17)$$

It can be seen that the maximum power using a one-step voltage compensation is equal to $P_{MAX} = \frac{2}{1+\gamma} P_{2MAX}$ where P_{2MAX} is the maximum power produced by the original series voltage inverting method given by [3] as $P_{2MAX} = \frac{I_P^2(1+\gamma)}{2\pi C_P \omega(1-\gamma)}$. Increasing the number of compensation steps causes further increase in P_{MAX}.

V. Cantilever Beam Geometry

In the previous section, it is assumed that a mechanical structure is utilized and the power conversion circuitry contributions are highlighted. In this section, the cantilever beam is studied. Although different mechanical structures have been presented [7-8] to transfer the vibration energy to piezoelectric material, the cantilever beam is more attractive for it's relatively low resonance frequencies and relatively high average strain for a given force input [7].

Different cantilever beam geometries are depicted in Fig. 6. It has been shown [7] that on trapezoidal beams, the strain is distributed more evenly along the beam as compared to rectangular beams. For the trapezoidal geometry more than twice the amount of energy (per unit volume PZT) can be generated than in the rectangular geometry. Further improvement in uniform distribution of strain can be achieved by taking into account the maximum tolerable strain at each point along the tapered beam.

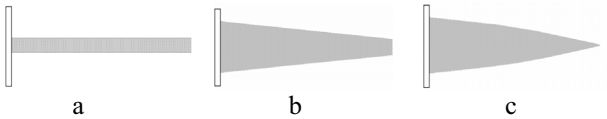

a b c

Fig. 6 (a) Rectangular beam; (b) Trapezoidal beam; (c) Tapered beam.

To reach this goal, a systematic tapered beam design is selected and presented herein. A tapered beam with a proof mass is depicted in Fig. 7. The function $f_1(x)$ describes the distance between cantilever beam's surface area and beam center and $f_2(x) = f_1(x) + t_b/2$ where t_b is the piezoelectric material thickness. An enlarged picture of the beam's length element is shown as the shaded area in Fig. 7b. From geometry, we know that

$$l^2 = (z+h)^2 + a^2 = b^2 + h^2 + 2zh \quad (18)$$

According to the Moment-Area Method [9]

$$z = \frac{M(x)}{EI(x)} \cdot \frac{\Delta x^2}{2} \quad (19)$$

where

$$M(x) = \frac{F}{EI(x)}(l_b + \frac{l_m}{2} - x) \quad (20)$$

with F is the force applied to the center of the proof mass, $I(x)$ is the moment of inertia given by

$$I(x) = 2(\frac{wt_P^3}{12} + wt_P f_2^2(x)) + \frac{2nwf_1^3(x)}{3} \quad (21)$$

Here w is the width of the beam (and piezoelectric), $n = \frac{E}{E_S}$ where E is the Young's modulus of the piezoelectric material and E_S is that of the metal beam.

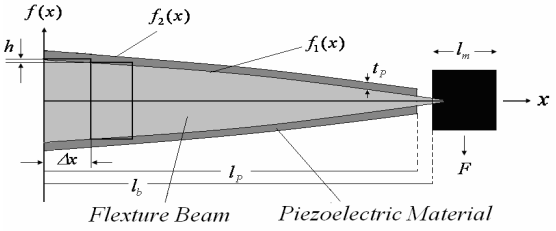

(a)

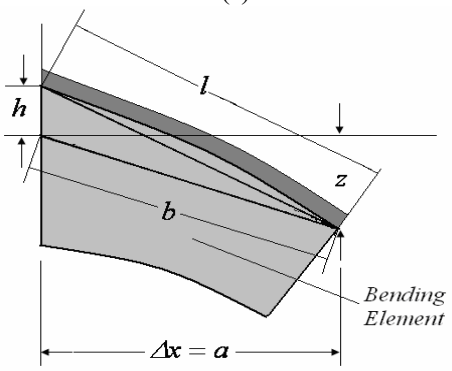

(b)

Fig. 7 (a)Tapered beam and its (b)bending element.

Also, from Fig. 7b we have

$$h \approx \left| f_2'(x) \right| \Delta x \text{ and } b = \Delta x(1 + \frac{M(x) f_2(x)}{EI(x)}) \quad (22)$$

Using (18) through (22), one has

$$l^2 = \Delta x^2[(1 + \frac{M(x) f_2(x)}{EI(x)})^2 + (\frac{df_2(x)}{dx})^2 + \frac{M(x)}{EI(x)} \frac{df_2(x)}{dx} \Delta x] \quad (23)$$

which can be approximated by

$$l^2 \approx \Delta x^2 \left[(1 + \frac{M(x) f_2(x)}{EI(x)})^2 + (\frac{df_2(x)}{dx})^2 \right] \quad (24)$$

Defining l_P' as the length of the unbent curvature underneath the piezoelectric material, we have the average strain along the beam as

$$\varepsilon_{ave} = \frac{l - l_P'}{l_P'} = \frac{1}{l_P'} \left[\int_0^{l_P} \sqrt{(1 + \frac{M(x) f_2(x)}{EI(x)})^2 + (\frac{df_2(x)}{dx})^2}\, dx - l_P' \right] \quad (25)$$

Also, the strain at each point along the beam can be obtained as

$$\varepsilon(x) = \frac{\sqrt{(1 + \frac{M(x) f_2(x)}{EI(x)})^2 + (\frac{df_2(x)}{dx})^2} - \sqrt{1 + (\frac{df_2(x)}{dx})^2}}{\sqrt{1 + (\frac{df_2(x)}{dx})^2}} . \quad (26)$$

Knowing from mechanics that $\varepsilon(x) = \frac{M(x) f_2(x)}{EI(x)}$, we have

$$\varepsilon(x) = \sqrt{1 + \frac{\varepsilon^2(x) + 2\varepsilon(x)}{1 + (\frac{df_2(x)}{dx})^2}} - 1 = \varepsilon_{CONST} \quad (27)$$

where ε_{CONST} is the desired constant strain along the beam.

Defining $\frac{\varepsilon^2(x) + 2\varepsilon(x)}{1 + (\frac{df_2(x)}{dx})^2} = K_1$ and after substituting for $\varepsilon(x)$, one is able to solve equation (27) for $\frac{df_2(x)}{dx}$ as

$$\frac{df_2(x)}{dx} = \sqrt{\frac{2EF(l_T - x)I(x) f_2(x) + F^2 (l_T - x)^2 f_2^2(x)}{K_1 E^2 I^2(x)} - 1} \quad (28)$$

where $l_T = l_b + l_m / 2$.

In order to solve (28), numerical approach has to be utilized. Also, an estimation of the applied force based on the vibration frequency and vibration amplitude is needed for a solution.

VI. Simulation and Experimental Results

The experimental setup consists of two 15cm steel cantilever beams, a rectangular and a tapered, both fixed on a shaker. The tapered beam has been designed at 32 equally apart points along the beam starting with $f_1(x) = 2\text{mm}$ at the fixed point using equation (28). The piezoelectric materials used are thin, flexible, strips of composite fibers with a laminate coating which are glued on the cantilever beam using epoxy. The material specifications are shown in Table 1. The test frequency and beam's free end vibration amplitude is 40Hz and 4mm for the rectangular beam and 47Hz and 2.5mm for the tapered one, respectively. The internal capacitance of the piezoelectric material was measured to be 2.8nF using a conventional multimeter. When the PZT leads are connected to the circuitry, the total capacitance seen from PZT terminals is not a constant but appears to be higher than 2.8nF due to capacitive effects of MOSFETs and measuring devices.

The polarization current I_P has been calculated using the equation $V_P = \frac{I_P}{C_P \omega}$ where V_P is the open circuit peak voltage. The parameter γ has been measured using voltage before and after inversion using oscilloscope and was not a constant. These values are given in Table .2 and Table .3.

Table.1 Piezoelectric material specifications. (Advanced Cerametrics Inc)

Specifications	**Values**
Fiber Type	PZT_5A
Dimensions	13.0cmX1.0cmX0.4cm
Avg. Actual Strain @ 3KVpp under 600Vdc bias(ppm)	1800
Operational Voltage Limits	-1500 to 2800
Weight	1.8grams
Dielectric Constant at 1kHz	1725
K_{33}	72%
D_{33}	380(10e-12m/V)
Young's Modulus	$6.6 \times 10^{10}\ \text{N/m}^2$

Table.2 Lab test specifications for the rectangular beam.

	Parallel Voltage Compensation	**Series Voltage Compensation**
Frequency	40Hz	40Hz
Beam's free end vibration amplitude	4mm	4mm
I_P	$76\mu A$	$76\mu A$
C_P	$2.8nF$	$2.8nF$
Total capacitance seen from PZT terminals	$3.7nF$	$4.7nF$
γ	<0.5	<0.5
Maximum Standard DC Power	1.4mW	1.4mW

Table.3 Lab test specifications for the tapered beam.

	Parallel Voltage Compensation	Series Voltage Compensation
Frequency	47Hz	47Hz
Beam's free end vibration amplitude	2.5mm	2.5mm
I_P	$170\mu A$	$170\mu A$
C_P	$2.8nF$	$2.8nF$
Total capacitance seen from PZT terminals	$3.9nF$	$6.2nF$
γ	<0.3	<0.3

In order to run the test for parallel inversion method, the circuit shown in Fig .8 is used along with a slightly different one for series inversion method.

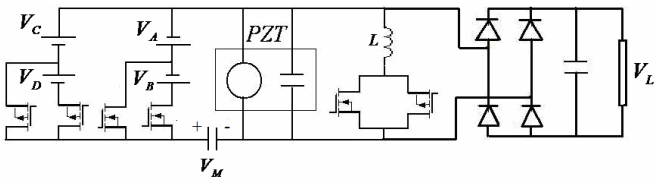

Fig. 8 Experimental test circuitry.

Instead of voltage sources V_A, V_B, V_C, and V_D the outputs of an adjustable flyback power converter have been used so that the compensated voltage can be adjusted. The voltage values $V_A + V_B$ and $V_C + V_D$ are kept slightly less than V_L to avoid direct charging of the rectifier capacitor. The transferred charge from the compensating power supplies to the PZT during each half-cycle has been measured using the change in voltage V_M at each compensation step. The compensating voltages V_A, V_B, V_C, and V_D have been measured using conventional multimeters. The net output power is defined as the difference between load power and injected power.

Using the beams described earlier and applying the mentioned test conditions, the simulation shows that the tapered beam has a near constant strain profile and is able to produce average strain twice the value as that of the rectangular beam for the same maximum applied strain. Fig. 9 shows the simulation results for the rectangular and tapered beam strains.

The experimental versus theoretical values for voltage compensation in parallel and series inversion methods are shown in Figs. 10 and 11, respectively, using the rectangular beam. According to the figures, experimental results match the theory with an acceptable accuracy at low voltages. However, at high voltages, they diverge due to the solid-state switches' off-state losses and input resistance of the measuring devices. It is shown that the voltage compensation method provides 14% increase in the harvested power in parallel voltage inversion and about 50% in series voltage inversion method.

For the tapered beam; on the other hand, Figs. 12 and 13 show larger difference between theoretical and experimental values. It is shown that the voltage compensation method provides 14% increase in the harvested power in parallel voltage inversion and about 75% in series voltage inversion method.

VII. Conclusions

Voltage inversion techniques are of the most effective methods to increase the scavenged power from mechanical vibrations using piezoelectric material subjected to alternating strain. The inversion process will not be efficient in a high power scavenger as there appears to be a significant voltage drop after voltage inversion which in turn decreases the efficiency of the harvesting method. Theoretical and experimental results show that by compensating the voltage after each inversion, the harvested power can be increased by 14% in the parallel inversion scenario and over 50% in the series inversion scenario compared to the case when such compensation is not used at all. We have also shown that a precisely designed tapered beam can produce twice as much strain and three times as much power as compared to a rectangular beam.

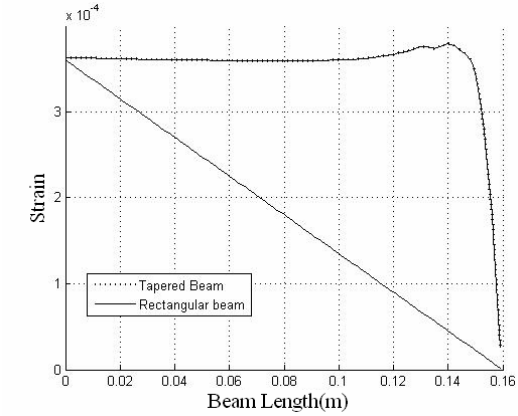

Fig. 9 Strain profile along rectangular and designed tapered beam.

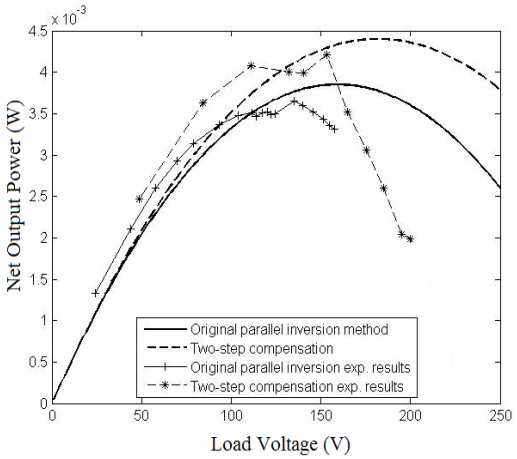

Fig. 10 Parallel inversion method; theoretical and experimental results using rectangular cantilever beam.

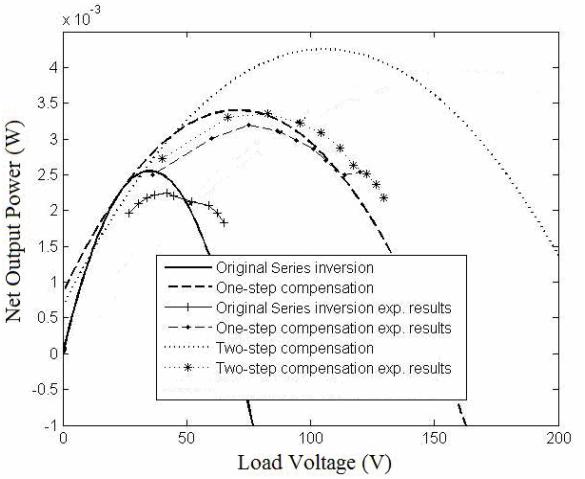

Fig.11 Series inversion method; theoretical and experimental results using rectangular cantilever beam.

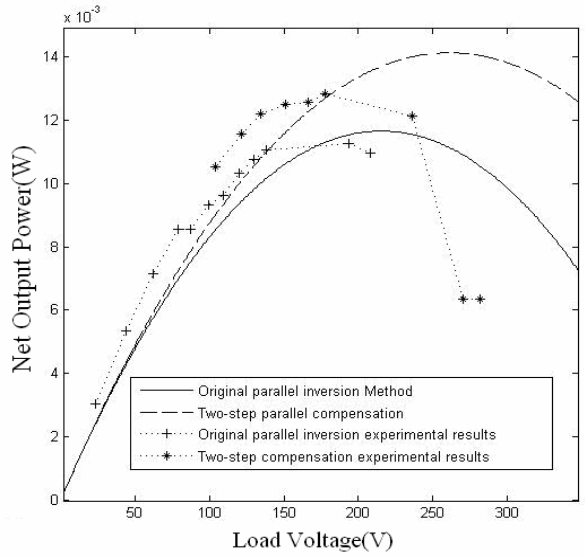

Fig. 12 Parallel inversion method; theoretical and experimental results using tapered cantilever beam.

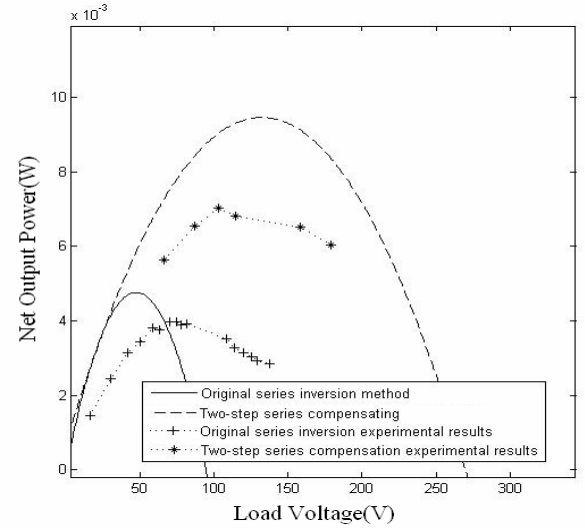

Fig. 13 Series inversion method; theoretical and experimental results using tapered cantilever beam.

REFERENCES

[1] V. Raghunathan, A. Kansal, J. Hsu, J. Friedman, and M. Srivastava, "Design Considerations for Solar Energy Harvesting Wireless Embedded Systems," *IEEE 4th International Symposium on IPSN*, pp. 457 – 462, 15 Apr 2005.

[2] G.K. Ottman, H.F. Hofmann, and G.A. Lesieutre, "Optimized piezoelectric energy harvesting circuit using step-down converter in discontinuous conduction mode." *IEEE Trans on Power Elect*, vol.18, no.2, pp.696-703, 2003.

[3] G.K. Ottman, H.F. Hofmann, A.C. Bhatt, and G.A. Lesieutre, "Adaptive Piezoelectric Energy Harvesting Circuit for Wireless Remote Power Supply," *IEEE Trans on Power Elec*, Vol 17, no. 5, pp. 669-676, 2002.

[4] D. Guyomar, A. Badel, E. Lefeuvre, and C. Richard, "Toward Energy Harvesting Using Active Materials and Conversion Improvement by Nonlinear Processing," *IEEE Transactions on Ultrasonics, Ferroelectrics, and Frequency Control*, vol. 52, no. 4, Apr 2005.

[5] A. Badel, B. Benayad, E. Lefeuvre, L. Lebrun, C. Richard, and D. Guyomar, "Single Crystals and Nonlinear Process for Outstanding Vibration-Powered electrical Generators," *IEEE Transactions on Ultrasonics, Ferroelectrics, and Frequency Control*, vol. 53, no. 4, April 2006.

[6] S. Roundy, P.K. Wright, and J. Rabaey, *Energy Scavenging for Wireless Sensor Networks with Special Focus on Vibrations*, Kluwer Academic Press, 2003.

[7] S. Roundy, E.S. Leland, J. Baker, E. Reilly, E. Lai, B. Otis, J.M Rabaey, P.K. Wright "Improving Power Output for Vibration-Based Energy Scavengers," Pervasive Computing, *Published by the IEEE CS and IEEE ComSoc 1536-1268*, pp. 28-36 January-March 2005.

[8] M. Ericka, D. Vasic, F. Costa, G. Poulain "Predictive Energy Harvesting from Mechanical Vibration Using a Circular Piezoelectric Membrane." *IEEE Ultrasonics Symposium*, pp. 946-949, *2005*.

[9] F.P. Beer and E.R. Johnston, *Mechanics of Materials,* McGRAW-HILL Book Company Europe, 1992